ChemSusChem

Research Article
doi.org/10.1002/cssc.202500343

Chemistry
Europe
European Chemical
Societies Publishing

www.chemsuschem.org

Hot Paper

Alloying Engineering of Defective Molybdenum Sulfide Basal Planes for Enhanced Borrowing Hydrogen Activity in the Thioetherification of Alcohols

Miriam Rodenes,[a] Darija Oštrić,[a] Santiago Martín,[b, c, d] Patricia Concepción,[a] Avelino Corma,*[a] and Iván Sorribes*[e]

The borrowing hydrogen thioetherification of alcohols over heterogeneous catalysts has emerged as an attractive and practical synthetic strategy to prepare thioethers from the perspective of green and sustainable chemistry. Developing efficient catalysts is the key to improve this carbon-sulfur (C—S) bond formation process. Herein, a novel catalyst, namely $\{Mo_{2.89}W_{0.11}S_4\}_n$, has been prepared by alloying engineering of its basal planes through an innovative synthetic methodology that makes use of isostructural building entities based on molybdenum and tungsten sulfide molecular complexes with M_3S_4 (M=Mo, W) cluster cores. Besides excellent activity and reus-

ability, $\{Mo_{2.89}W_{0.11}S_4\}_n$ is of broad scope, enabling the conversion of structurally diverse thiols and primary as well as secondary alcohols into thioethers. A set of characterizations, in combination with catalytic results, reveal that the catalytic activity of $\{Mo_{2.89}W_{0.11}S_4\}_n$ for this relevant transformation arises from the presence of multiple-type active centers in the defective basal planes of this alloyed catalyst. More specifically, coordinatively unsaturated sulfurs and metal atoms with Lewis basic and Lewis acid properties, respectively, are proposed to be the active sites involved in the borrowing hydrogen mechanism.

Introduction

The construction of C—S bonds has drawn great interest in organic synthesis due to sulfur-containing compounds have important applications in biological and material science fields, as well as in the pharmaceutical and agrochemical industries.[1–9] In particular, thioethers constitute the vital component of many drugs and biologically active compounds.[10–16] In recent years, the borrowing hydrogen thioetherification of alcohols has

become an attractive and practical strategy of high significance from the green and sustainable chemistry point of view.[17–19] In this one-pot domino sequence, the alcohol is dehydrogenated to an aldehyde or ketone intermediate, which reacts with the thiol resulting in a transient hemithioacetal that is in-situ reduced using the previously released hydrogen-derived species to yield the desired thioether with minimal waste generation (Scheme 1a).[20–24]

Traditionally, the synthesis of thioethers[25] is accomplished through the condensation of metal alkyls or aryl thiolates with alkyl halides, cross-coupling reactions of organic halides with thiols,[4,26–39] metal-catalyzed hydrothiolations of unsaturated carbon–carbon bonds,[32,40–55] or activation of alcohol electrophiles via Brønsted or Lewis acid catalysis.[14,56–65] Compared to these synthetic procedures, the borrowing hydrogen methodology using thiols and alcohols, which are an important part of our chemical feedstocks, offers compelling benefits. Among others, shortcomings associated with the formation of inorganic waste, low availability of starting materials, regioselectivity issues, and reactivity limitations ascribed to the poor leaving character of the hydroxyl functionality, are advantageously avoided.

The pioneering work on the borrowing hydrogen thioetherification of alcohols involves the use of a heterogeneous catalyst based on palladium nanoparticles supported on high-surface area magnesium oxide (MgO).[20] Application of this catalyst allowed the preparation of thioethers along with the formation of disulfides. In the following years, with the aim of avoiding the use of precious metals, some of us developed cobalt-molybdenum sulfide unsupported materials,[66–67] and established them as excellent catalysts for the construction of C—S bonds in thioethers via the borrowing hydrogen strategy

[a] Instituto de Tecnología Química, Universitat Politècnica de València-Consejo Superior de Investigaciones Científicas (UPV-CSIC), València, Spain

[b] Instituto de Nanociencia y Materiales de Aragón (INMA), Consejo Superior de Investigaciones Científicas (CSIC)-Universidad de Zaragoza, Zaragoza, Spain

[c] Departamento de Química Física, Facultad de Ciencias, Universidad de Zaragoza, Zaragoza, Spain

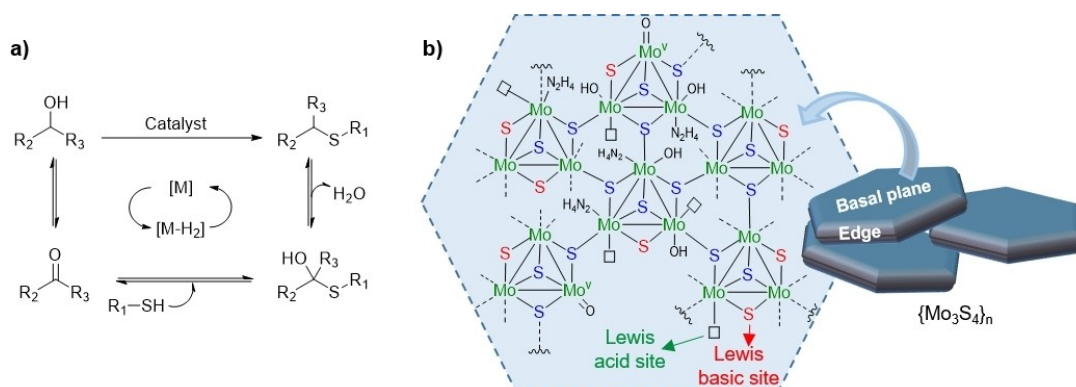[d] Laboratorio de Microscopias Avanzadas (LMA), Universidad de Zaragoza, Zaragoza, Spain

[e] Institute of Advanced Materials, Universitat Jaume I, Castelló de la Plana, Spain

Correspondence: Prof. Dr. Avelino Corma, Instituto de Tecnología Química, Universitat Politècnica de València-Consejo Superior de Investigaciones Científicas (UPV-CSIC), Av. de los Naranjos, s/n, 46022 València, Spain.
Email: acorma@itq.upv.es

Prof. Dr. Iván Sorribes, Institute of Advanced Materials, Universitat Jaume I, Av. Vicent Sos Baynat, s/n, 12071 Castelló de la Plana, Spain.
Email: isorribe@uji.es

Supporting Information for this article is available on the WWW under https://doi.org/10.1002/cssc.202500343

ChemSusChem

Research Article
doi.org/10.1002/cssc.202500343

Chemistry
Europe
European Chemical
Societies Publishing

Scheme 1. a) Borrowing hydrogen mechanism for the thioetherification of alcohols. b) Molecular cluster-derived defective basal plane of $\{Mo_3S_4\}_n$.

by the reaction of thiols (including hydrogen sulfide) with primary and secondary alcohols.[68] Recently, we have demonstrated that non-promoted molybdenum sulfides catalyze more efficiently this reaction.[69] The key to successful catalysis relies on the use of a catalyst that presents a high density of active sites in the basal planes, which are mostly inactive in molybdenum disulfide (MoS_2)-type catalysts (Scheme 1b).[70] In the meantime, the borrowing hydrogen strategy were also applied for the S-benzylation/alkylation of dithiocarbamates with alcohols using hydroxyapatite-supported copper nanoparticles as the catalyst.[19]

For decades, great efforts have been devoted to improve the activity of MoS_2-derived materials for thermal-, electro-, and photocatalytic processes.[71–79] Traditional strategies to improve the catalytic activity of MoS_2 are based on the use of metal promoters (commonly Co or Ni). These metals tend to be adsorbed at the edges of its lamellar structure leading to the formation of Co(Ni)-Mo—S structures with metal-like electronic states that are proposed as the potential actives sites where organic molecules are activated.[80–87] Additionally, these promoters also facilitate the formation of more actives centers at the edges in the form of coordinatively unsaturated sites (CUS).[88]

Since it was postulated that active sites of MoS_2 are mainly located at the edges while basal planes are catalytically inert,[89–92] other approaches that avoided the use of promoters were focused on the design of edge-rich nanomaterials to maximally expose the active edge sites.[93–94] However, the structural configuration of MoS_2 implies a low perimeter-to-basal plane area ratio,[95] so these materials exhibit limited inherent catalytic activity compared to those in which the basal planes are active. Interestingly, disorder engineering offers compelling advantages to this issue due to disordered structures of MoS_2-derived materials usually possess a high density of active sites in the basal planes.[73] In essence, the bottom-up synthetic strategy we previously reported follows this approach to engineer sulfur-deficient and sulfur-enriched MoS_2-type nanomaterials from molecular complexes with Mo_3S_4 and Mo_3S_7 cluster cores, respectively.[70,96] The resulting defective molybdenum sulfides preserve the specific atomic arrangement of the cluster motif precursor, a fact that leads to the

presence of proliferated structural defects on the naturally occurring edge position and along the commonly non-active basal planes. Advantageously, this allows their useful application as heterogeneous catalysts for chemical process intensification in fine chemical synthesis[69–70] and for electrocatalysis.[96] In particular, the peculiar structure configuration of the Mo_3S_4 cluster units provides, upon their self-assembly, a defective nanomaterial, known as $\{Mo_3S_4\}_n$, that displays unsaturated bridging sulfide ligands and molybdenum atoms with Lewis basic and Lewis acid character, respectively (Scheme 1b). Importantly, both unsaturated centers proved to be key active sites for successful borrowing hydrogen thioetherification of alcohols.[69]

Nevertheless, the performance of the catalyst $\{Mo_3S_4\}_n$ for the target reaction could be further improved, reason that kept encouraging our search for new synthetic strategies to optimize their surface structure at the nanoscale. On the basis of a good knowledge on the reaction kinetics governing the borrowing hydrogen process in the presence of this catalyst, we envisioned that its modification by introducing a second metal with different electronic properties would be advantageous for improving its catalytic activity. In this context, disorder engineering by alloy formation is an established methodology to modulate the electronic and catalytic properties of materials.[73,97–98] In this contribution, an alloyed bimetallic material, named $\{Mo_{2.89}W_{0.11}S_4\}_n$, is prepared by combining isostructural building entities based on molybdenum and tungsten sulfide molecular complexes with M_3S_4 (M=Mo, W) cluster cores. We demonstrate that the catalytic activity of the alloyed material for the borrowing hydrogen thioetherification of alcohols can be controlled as a function of the tungsten content to exhibit higher activity than that of the monometallic catalyst $\{Mo_3S_4\}_n$. According to in situ infrared spectroscopy studies, this improvement in the catalytic activity can be attributed to the presence of multiple-type active centers, which are present in the defective basal planes of the alloyed catalyst. Furthermore, we also show that application of this alloyed catalyst allows the synthesis of a broad range of thioethers from structurally diverse thiols and primary as well as secondary alcohols.

Results and Discussion

### Kinetic Study for the Catalyst {Mo₃S₄}ₙ

It is generally accepted that the borrowing hydrogen thioetherification of alcohols proceeds via the two elementary steps shown in Scheme 2a: 1) the alcohol dehydrogenation to the aldehyde, and 2) the reductive thiolation of the aldehyde to afford the final thioether via a hemithioacetal intermediate, which reacts rapidly in route.[20–24] As previously reported,[20] two kinetic rate expressions can be proposed (Eq. 1 and 2, Scheme 2b) when it is assumed that either of the two reaction steps can be the rate-determining step while the other is in equilibrium, and when the rate of change of the concentration of the aldehyde intermediate is considered to be constant. From these kinetic equations, it is possible to deduce that the study of the effect of the initial concentration of the reactants on the initial reaction rate should allow obtaining the rate-determining step because the thiol is involved in the reductive thiolation but not in the alcohol dehydrogenation step. Notably, the elucidation of the rate-determining step of the overall process is crucial to know which step of the reaction needs to be accelerated and, hence, what modifications could be undertaken on the catalyst to boost its activity.

To investigate the kinetic behavior of the catalyst {Mo₃S₄}ₙ on the borrowing hydrogen thioetherification of alcohols, we selected the alkylation of benzenethiol (**1a**) with benzyl alcohol (**2a**) to obtain benzyl phenyl sulfide (**3aa**) as the benchmark reaction. The experiments were performed under the optimum conditions for this catalyst (toluene, 180 °C, N₂ atmosphere), which also involve a catalyst pre-activation treatment (180 °C, 2 h, vacuum conditions) carried out before running the catalytic experiments with the aim to create vacant coordination sites around the Mo atoms (i.e. Lewis acid sites) at a higher extent.[69] Then, the reaction profiles were obtained at different concentrations of either **1a** or **2a** while keeping the concentration of the other one constant (Figures S1–S2). At the beginning, the desired thioether **3aa** and phenyl disulfide (**4a**) are simultaneously formed, but the concentration of the by-product **4a** reaches a maximum and begins to decrease. This observation indicates that, in the presence of the catalyst {Mo₃S₄}ₙ, the
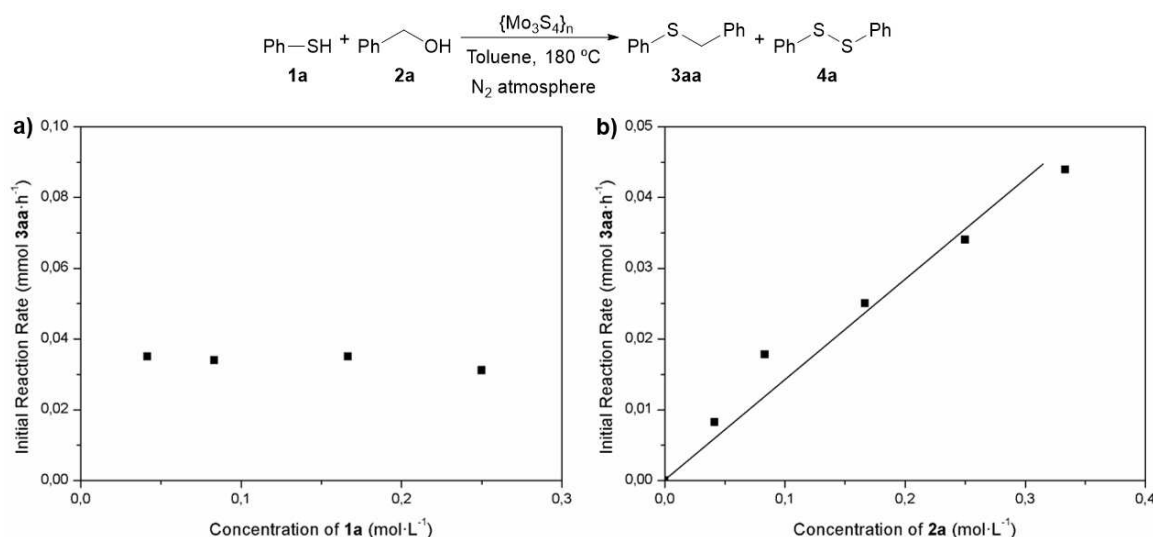
disulfide bond in **4a** is firstly formed and later reduced to form the starting thiol **1a** again. Importantly, no accumulation of the aldehyde intermediate was detected along these kinetic experiments, thus confirming that the steady state approximation considered to propose the kinetic rate expressions (Eqs. 1 and 2) is correctly applied. As shown in Figure 1, the initial reaction rates for the formation of **3aa**, obtained from the measured reaction profiles (Figures S1–S2), increases linearly with the concentration of the alcohol **2a** while remains practically non-affected when modifying the concentration of the thiol **1a**. This kinetic behavior reveals that the rate-determining step for the borrowing hydrogen thioetherification of benzyl alcohol (**2a**) with benzenethiol (**1a**) in the presence of {Mo₃S₄}ₙ is not the reductive thiolation step, but the dehydrogenation of the alcohol, since the reaction rate does not depend on the concentration of the thiol. The direct conclusion from these kinetic results is that the modification of {Mo₃S₄}ₙ to enhance its activity should be aimed at increasing its alcohol dehydrogenation activity while maintaining its transfer hydrogenation efficiency. On that basis, we decided to prepare molybdenum- and tungsten-based bimetallic nanomaterials expecting that alloyed and defective basal planes of these nanomaterials, featuring multiple types of active centers, could constitute an advanced catalytic platform for enhanced borrowing hydrogen activity in the thioetherification of alcohols.

Designing a Catalyst with Higher Catalytic Activity: Preparation and Catalytic Activity of Bimetallic {(MoW)ₓSᵧ}ₙ Catalysts

In recent years, we have been engaged in the preparation of defective molybdenum sulfide nanomaterials through a synthetic methodology that makes use of well-defined molecular complexes as precursors.[70,96] Concretely, the nanomaterial {Mo₃S₄}ₙ was engineered from a molecular complex comprising three metal atoms disposed in an equilateral triangular arrangement, an apical sulfur atom (Mo₃-μ₃-S), and three bridging sulfur ligands (Mo₂-μ-S). Moreover, labile triphenylphosphine and halide ligands as well as solvent molecules occupy the outer coordination sphere of the metal atoms. The intercluster self-
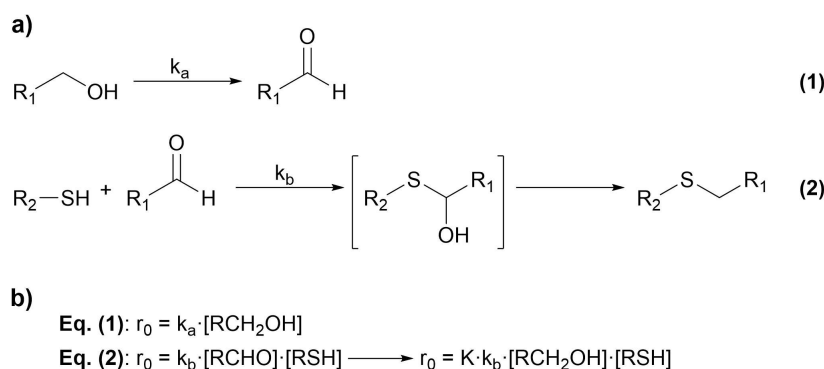
Scheme 2. a) Reaction steps for the borrowing hydrogen thioetherification of alcohols. b) Kinetic rate expressions obtained by considering that either the first step or the second step is the rate-determining one. Kₐ and k_b are the kinetic constants of steps (1) and (2), respectively; K is the steady-state constant obtained by applying the steady-state approximation for the aldehyde intermediate.

a)

R₁—CH₂—OH $\xrightarrow{k_a}$ R₁—CHO (1)

R₂—SH + R₁—CHO $\xrightarrow{k_b}$ [R₂—S—CH(OH)—R₁] ⟶ R₂—S—CH₂—R₁ (2)

b)

Eq. (1): $r_0 = k_a \cdot [RCH_2OH]$

Eq. (2): $r_0 = k_b \cdot [RCHO] \cdot [RSH] \longrightarrow r_0 = K \cdot k_b \cdot [RCH_2OH] \cdot [RSH]$

ChemSusChem

Research Article
doi.org/10.1002/cssc.202500343

Chemistry
Europe
European Chemical
Societies Publishing

Figure 1. Kinetic studies for the borrowing thioetherification of **2a** with **1a** in the presence of $\{Mo_3S_4\}_n$. **a)** Initial reaction rate at different concentration of **1a**. **b)** Initial reaction rate at different concentration of **2a**. Reaction conditions: 0.25 mmol **1a** for b), 0.75 mmol **2a** for a), $\{Mo_3S_4\}_n$ (30 mg), toluene (3 mL), *n*-hexadecane as an internal standard (0.1 mmol), 10 bar N_2, 180 °C.

assembly of this building entities, by which $\{Mo_3S_4\}_n$ is formed, is a process driven by reduction with hydrazine and involves the nucleophilic attack from the bridging sulfur ligands to the outer coordination sites of metal atoms. Taking advantage of the isostructural arrangement of the tungsten sulfide molecular complex with W_3S_4 cluster core (Figure 2a), we envisioned the possibility of preparing bimetallic molybdenum- and tungsten-based nanomaterials of general formula $\{(MoW)_xS_y\}_n$. Thus, we adapted our previously reported preparation methodology by combining molecular complexes with Mo_3S_4 and W_3S_4 cluster cores to obtain nanomaterials in which the mole ratios of the precursors were chosen so that nominally the W/Mo mole ratios were 0.03, 0.06, 0.14, 0.33, and 1. For comparison, the monometallic nanomaterial $\{Mo_3S_4\}_n$ and the one consisting only of tungsten ($\{W_xS_y\}_n$) were also synthetized under the same preparation conditions.

The nanomaterials prepared with different tungsten content were structurally characterized by powder X-ray diffraction (XRD). Because of the isostructural character of both molecular cluster precursors, the prepared nanomaterials are expected to exhibit almost the same lattice constants, resulting in the overlapping of diffraction peaks. In fact, the XRD patterns of all nanomaterials show the same broad diffraction peaks as those found in $\{Mo_3S_4\}_n$ (Figure 2b). Interestingly, the peak associated with the (002) plane is slightly shifted from 13.1 to 14.5° in tungsten-containing nanomaterials, which can tentatively ascribed to the formation of alloyed structures. Furthermore, the XRD diffraction patterns also exhibit the presence of peaks at 2θ values of 40.3, 58.3, 73.2, and 87.0° that can be indexed to the (110), (200), (211), and (220) planes, respectively, of the cubic phase of W^0 in agreement with the JCPDS database (PDF card 00–004-0806). These diffraction peaks become progressively noticeable and sharper with the increase of the W_3S_4 cluster precursor in the nanomaterial preparation, which means that

part of this precursor is reductively decomposed to W^0 by hydrazine in the preparation step.

With these materials in hand, we evaluated their catalytic performance for the borrowing hydrogen thioetherification of alcohols by comparing the initial reaction rates obtained for the model reaction between the thiol **1a** with the alcohol **2a** to obtain the thioether **3aa**. By plotting the initial reaction rates for the formation of **3aa** obtained for the catalysts with increasing molar ratios of W/Mo, a volcano-shaped curve with the maximum at W/Mo of 0.06 was observed (Figure 2c and Figure S3). To the best of our knowledge, this is the highest catalytic activity (measured by the initial reaction rate normalized to the moles of metal) reported to date for the above-mentioned reaction catalyzed by the state-of-the-art noble metal-free heterogeneous catalysts (Figure S4). Considering that the kinetic of the overall reaction in the presence of the monometallic catalyst $\{Mo_3S_4\}_n$ is determined by the alcohol dehydrogenation step, the increase of the catalytic activity upon tungsten incorporation could be directly associated with a higher performance of these catalysts in carrying out such a step. If this is so, it may be that the most active catalyst catalyzes so fast the alcohol dehydrogenation reaction that this will be not the slowest reaction step anymore, but the reductive thiolation between the aldehyde intermediate and the thiol. Indeed, the series of kinetic experiments, in which the initial concentration of benzenethiol (**1a**) was kept constant while varying the initial concentration of benzyl alcohol (**2a**) and vice versa, revealed that the initial reaction rate for the formation of **3aa** in the presence of the catalyst $\{(MoW)_xS_y\}_n$-0,06 depends on both the alcohol and the thiol (Figure 3 and Figures S5–S6).

ChemSusChem

Research Article
doi.org/10.1002/cssc.202500343

Chemistry
Europe
European Chemical
Societies Publishing
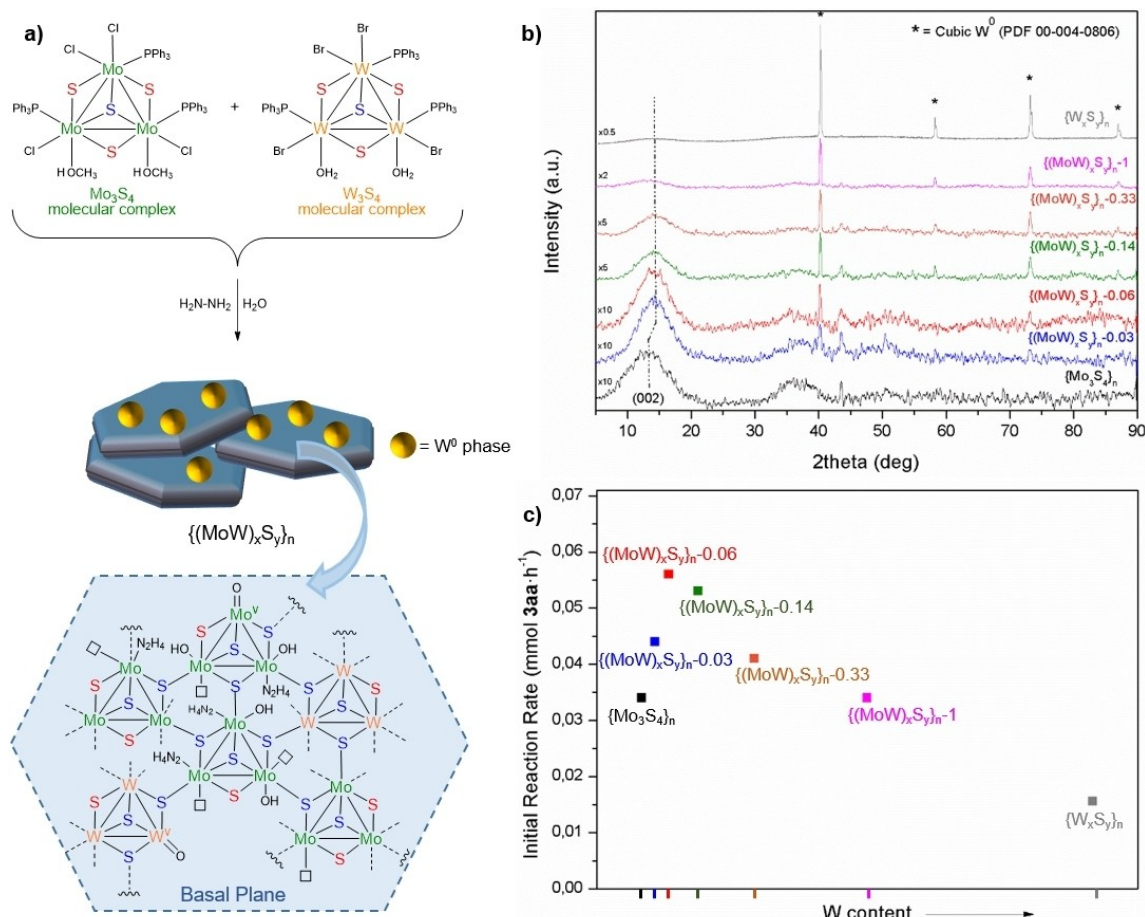
Figure 2. a) Synthesis of nanomaterials $\{(MoW)_xS_y\}_n$ from molecular complexes with MS_4 (M=Mo, W) cluster cores. **b)** XRD diffraction patterns of nanomaterials $\{Mo_3S_4\}_n$, $\{(MoW)_xS_y\}_n$-Z (Z=W/Mo mole ratio), and $\{W_xS_y\}_n$. **c)** Initial reaction rates for the formation of **3aa** in the borrowing thioetherification of **2a** with **1a** in the presence of $\{Mo_3S_4\}_n$, $\{(MoW)_xS_y\}_n$-Z (Z=W/Mo mole ratio), and $\{W_xS_y\}_n$ as catalysts. Reaction conditions: **1a** (0.25 mmol), **2a** (0.75 mmol), catalyst (30 mg), toluene (3 mL), n-hexadecane as an internal standard (0.1 mmol), 10 bar N_2, 180 °C.
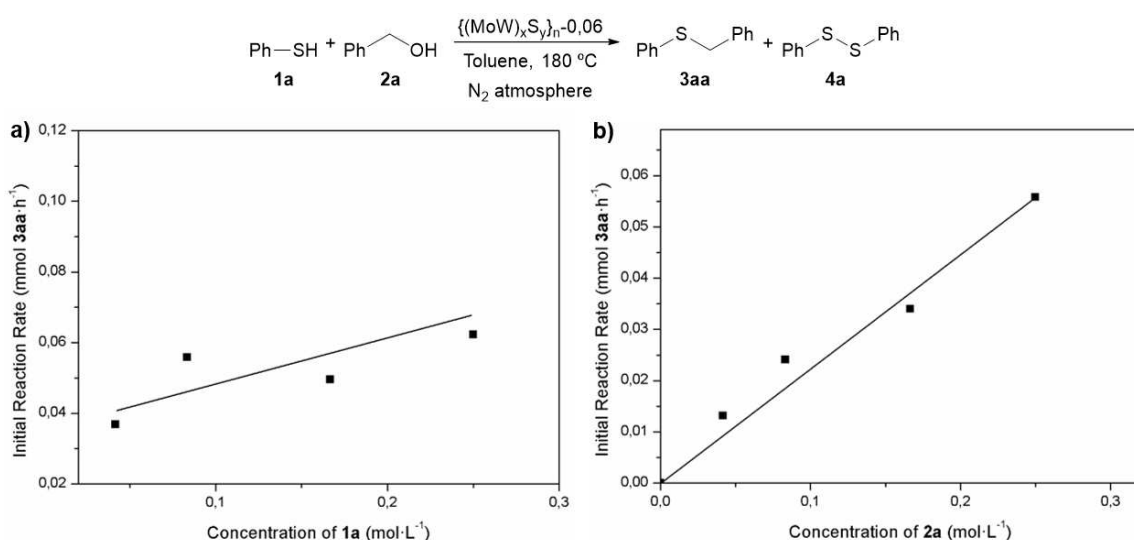
Figure 3. Kinetic studies for the borrowing thioetherification of **2a** with **1a** in the presence of $\{(MoW)_xS_y\}_n$-0.06. **a)** Initial reaction rate at different concentration of **1a**. **b)** Initial reaction rate at different concentration of **2a**. Reaction conditions: 0.25 mmol **1a** for b), 0.75 mmol **2a** for a), $\{(MoW)_xS_y\}_n$-0.06 (30 mg), toluene (3 mL), n-hexadecane as an internal standard (0.1 mmol), 10 bar N_2, 180 °C.

ChemSusChem

Research Article
doi.org/10.1002/cssc.202500343

Chemistry
Europe
European Chemical
Societies Publishing

Characterization of the Catalyst {(MoW)$_x$S$_y$}$_n$-0,06 ({Mo$_{2.89}$W$_{0.11}$S$_4$}$_n$)

Next, the most active catalyst ({(MoW)$_x$S$_y$}$_n$-0.06) was further characterized. Inductively coupled plasma optical emission spectrometry (ICP-OES) measurements were combined with combustion elemental analyses in order to determine its metal and sulfur composition. A lower W/Mo mole ratio was obtained experimentally in comparison with the theoretical value (0.04 *versus* 0.06, respectively), which is likely due to the partial decomposition of the W$_3$S$_4$ molecular precursor to W^0 by hydrazine treatment during the material preparation, as revealed by XRD spectroscopy. Despite this, a negligible sulfur loss occurred other than that caused by the W$_3$S$_4$ molecular cluster decomposition because the molar ratio S/(Mo + W) was determined to be 1.33. Therefore, this bimetallic molybdenum- and tungsten-based nanomaterial (i.e. {(MoW)$_x$S$_y$}$_n$-0.06) can be defined and hereinafter named as {Mo$_{2.89}$W$_{0.11}$S$_4$}$_n$. Furthermore, the combustion elemental analysis also revealed that {Mo$_{2.89}$W$_{0.11}$S$_4$}$_n$ displays some nitrogen content (10.2%), which most likely originates from hydrazine ligands coordinated to metal atoms. This nitrogen content was considerably reduced to 2.8% under the catalyst pre-activation treatment carried out before running the catalytic experiments (see the experimental section for further details), through which the catalyst is expected to be furnished with sulfhydryl species (S–H) and coordinatively unsaturated metal atoms with Lewis acid character, as previously reported for the monometallic nanomaterial {Mo$_3$S$_4$}$_n$.[69]

The Raman spectrum of {Mo$_{2.89}$W$_{0.11}$S$_4$}$_n$ exhibits the Raman vibration bands characteristic of both trimetallic sulfide units, including those from metallic bonds (ν(M–M)) at 125–230 cm^{-1}, molybdenum and tungsten sulfide bonds (ν(M–S)) at 240–384 cm^{-1}, bridging sulfur ligands at 430 and 434 cm^{-1} (ν(μ-S–M); M≡Mo and W, respectively), and the apical sulfur atom (ν(μ_3-S–M)) at 444 cm^{-1} (Figure 4a).[99–100] Interestingly, compared with the monometallic nanomaterial {Mo$_3$S$_4$}$_n$, a noticeable broadening of the peak center associated with the bridging sulfur ligands (ν(μ-S–M)) is observed upon the introduction of tungsten. This is because in {Mo$_{2.89}$W$_{0.11}$S$_4$}$_n$ the broadened Raman peak comprises bridging sulfur ligands of both molybdenum and tungsten cluster units, which differ to each other by 4 cm^{-1}. In addition, broad Raman bands centered at around 710 and 880 cm^{-1}, respectively associated to the presence M^{IV}−OH and M^V=O species (M≡Mo, W), were also discerned.[99,101–102] These species result from the partial oxidation of the cluster metal core of the constituent units (see Figure 2a).
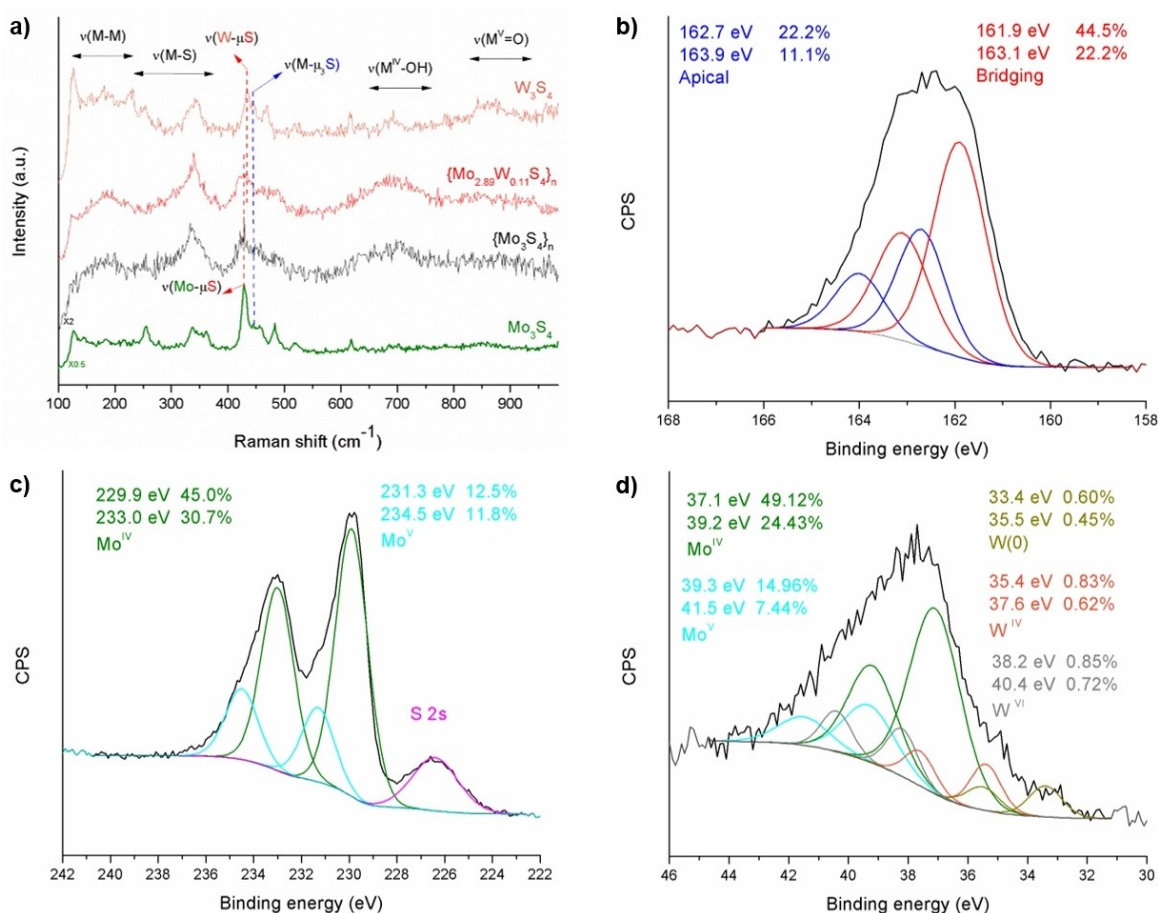
Figure 4. a) Raman spectra of the nanomaterials {Mo$_3$S$_4$}$_n$ and {Mo$_{2.89}$W$_{0.11}$S$_4$}$_n$, and of the molecular precursors with M$_3$S$_4$ (M≡Mo, W) cluster cores. XPS spectra of S 2p (**b**), Mo 3d (**c**), and W 4f (**d**) core levels of the nanomaterial {Mo$_{2.89}$W$_{0.11}$S$_4$}$_n$.

ChemSusChem

Research Article
doi.org/10.1002/cssc.202500343

**Chemistry
Europe**
European Chemical
Societies Publishing

X-ray photoelectron spectroscopy (XPS) was used to get more information about the chemical composition of the catalyst $\{Mo_{2.89}W_{0.11}S_4\}_n$. No peaks of chlorine, bromine or phosphorus could be found in the XPS survey spectrum (Figure S7), indicating that halogens and triphenylphosphine ligands are completely removed with the intercluster self-assembly by which the catalyst is formed. Conversely, the nitrogen peak was clearly detected, which supports that some hydrazine molecules must remain coordinated to metal atoms. The high-resolution S 2p core-level spectrum displays a broad signal, which could be fitted into the two sets of doublets characteristic of the molecular cluster sulfide M_3S_4 (M=Mo, W) assembly (Figure 4b).[70] The doublet at binding energies (BEs) of 161.9 and 163.0 eV, whose components are respectively associated to the spin–orbit splitting of S $2p_{3/2}$ and S $2p_{1/2}$ orbitals, corresponds to the unsaturated bridging sulfur ligands (M_2-μ-S; red in Figure 2a). The other doublet at 162.5 and 163.7 eV belongs to the two types of saturated sulfurs, *i.e.* the original apical ones and the sulfur ligands linking different cluster units (M_3-μ_3-S and M_2-μ-S—M, respectively; blue color in Figure 2a). It is worth mentioning that, due to the intercluster self-assembly by which the catalyst $\{Mo_{2.89}W_{0.11}S_4\}_n$ is formed, the signal deconvolution into the two doublets resulted in a lower area ratio of bridging to saturated sulfur ligands (67:33) compared to the theoretical value expected for the molecular cluster precursors (75:25).

The signal deconvolution in the high-resolution Mo 3d energy-level spectrum denotes the presence of two distinct chemical Mo species (Figure 4c). More specifically, the doublet at BEs of 229.9 and 233.0 eV corresponding to the Mo $3d_{5/2}$ and Mo $3d_{3/2}$ orbitals, respectively, are associated to Mo(IV) species, whereas the other two peaks at 230.9 and 234.4 eV are ascribed to the presence of molybdenum oxysulfides ($Mo^vO_xS_y$).[99]

Determination of W-oxidation states in heterobimetallic molybdenum sulfides is challenging because the BEs of tungsten and molybdenum species in the W 4f and Mo 4p regions, respectively, are similar in both cases (Figure 4d). First, the area ratio between the two doublets corresponding to Mo(IV) and $Mo^vO_xS_y$ species was set according to the values previously established for the Mo 3d region. Then, the signal could be further deconvoluted and fitted into three additional doublet peaks, each of them characteristic of the spin–orbit splitting of W $4f_{7/2}$ and W $4f_{5/2}$ orbitals. The doublets at 35.4/

37.6 eV and 38.2/40.4 eV are associated with the presence of W(IV) and tungsten oxysulfides species ($W^vO_xS_y$), respectively, whereas the doublet at BEs of 33.4/35.5 eV is ascribed to W^0. Interestingly, all the peaks of the tungsten species are slightly shifted to higher BEs compared to the values found for the W_3S_4 molecular cluster complex (Figure S8) and in the literature data for W^0.[103] This shift is most likely due to the high electronic interaction between the tungsten species and the surrounding Mo_3S_4-derived extended structure.[104]

Transmission electron microscopy (TEM) images taken at various magnifications show that $\{Mo_{2.89}W_{0.11}S_4\}_n$ consists of randomly agglomerated nanosheets of amorphous nature exhibiting irregular and disordered basal planes (Figure 5a–c). Although the presence of the W^0 phase was inferred by XRD and XPS measurements, however, metal nanoparticles of W^0 were not visualized, suggesting that these are sub-nanometer in size and/or are highly dispersed within the nanomaterial $\{Mo_{2.89}W_{0.11}S_4\}_n$. The component distribution was determined by energy-dispersive X-ray spectroscopy (EDS) elemental mapping studies (Figure 5d), which revealed that this nanomaterial is mostly constituted by molybdenum, sulfur, and tungsten to a lesser extent, all of them homogeneously distributed over the entire sample. Additionally, nitrogen and oxygen elements were also detected in agreement with XPS, Raman, and elemental analysis characterizations.

Catalyst Recycling Experiments and Characterization

In order to demonstrate the stability and recyclability of the catalyst $\{Mo_{2.89}W_{0.11}S_4\}_n$, it was reused several times for the model reaction between the thiol **1a** with the alcohol **2a**. No catalyst deactivation occurred along the reaction runs, as shown in Figure 6a and Figure S9, which depict the catalyst recycling experiments at incomplete reaction times (2 h) and the initial reaction rates for the formation of **3aa** obtained from each reaction run, respectively. The XRD pattern of the catalyst after the fifth run exhibits more noticeable and sharper peaks associated with the cubic phase of W^0 than the fresh catalyst (Figure S10). This result confirms the presence of W^0 in a larger particle size. Indeed, an accurate examination of the HRTEM images obtained for the five-times-used catalyst ($\{Mo_{2.89}W_{0.11}S_4\}_n$-R) allows us visualizing the characteristic lattice
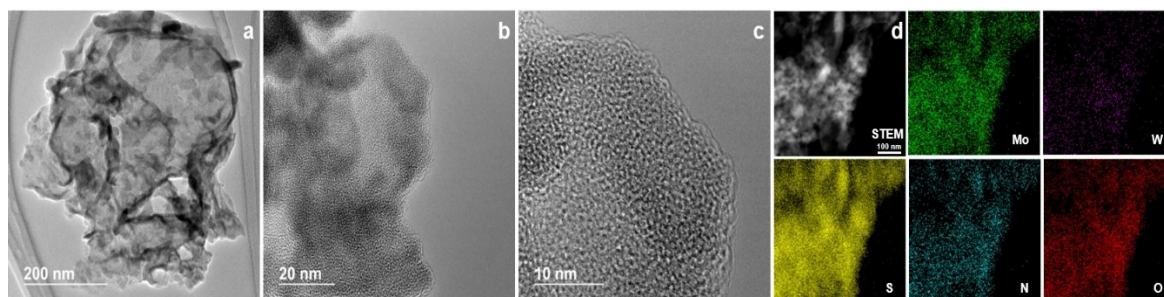
Figure 5. Electron microscopy characterization of $\{Mo_{2.89}W_{0.11}S_4\}_n$. TEM (**a**) and High-resolution TEM (HRTEM) (**b**,**c**) micrographs. **d**) High-angle annular dark-field scanning transmission electron microscopy (HAADF-STEM) image and EDS elemental mapping of Mo, W, S, N, and O.
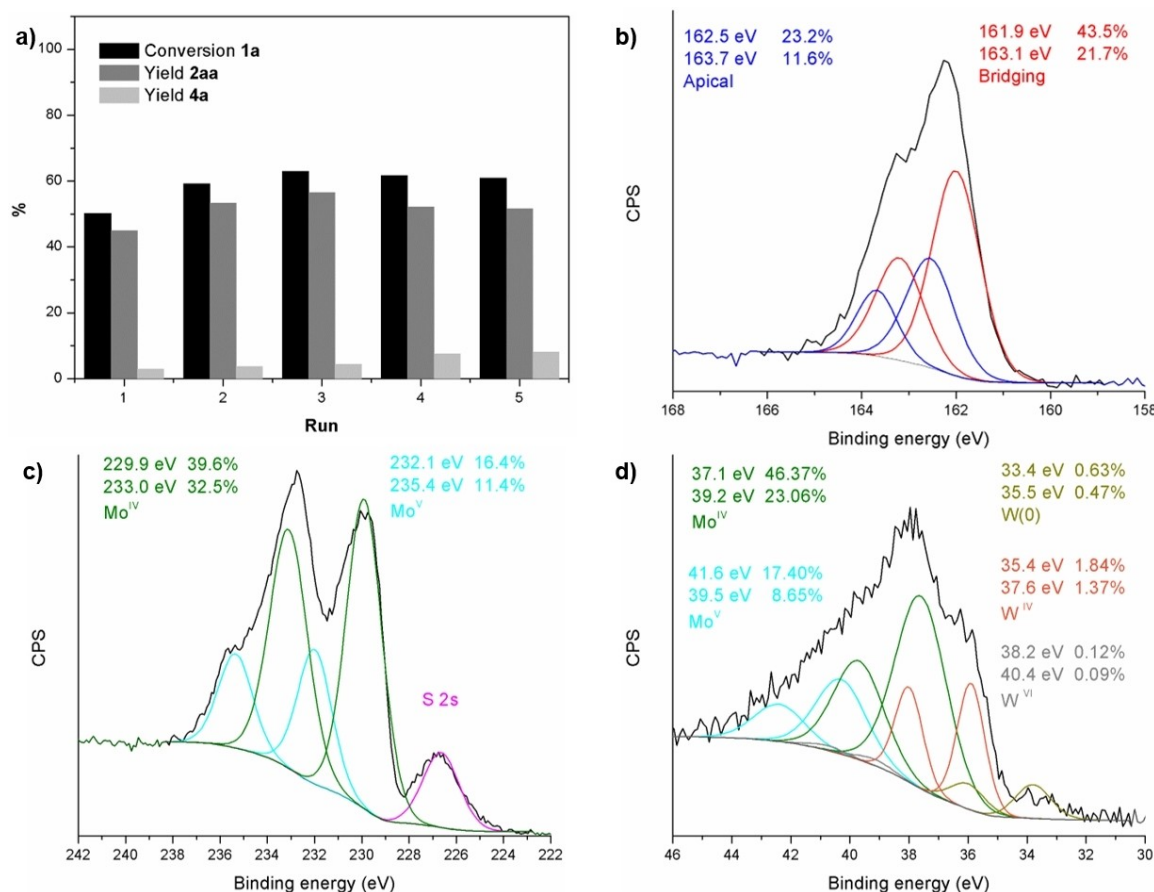
Figure 6. a) Recycling experiments of the catalyst $\{Mo_{2.89}W_{0.11}S_4\}_n$ for the thioetherification of **2a** with **1a**. Reaction conditions: 0.25 mmol **1a**, 0.75 mmol **2a**, $\{Mo_{2.89}W_{0.11}S_4\}_n$ (34 mg), toluene (3 mL), n-hexadecane as an internal standard (0.1 mmol), 10 bar N_2, 180 °C, 2 h. XPS spectra of S 2p (**b**), Mo 3d (**c**), and W 4f (**d**) core levels of the recycled catalyst $\{Mo_{2.89}W_{0.11}S_4\}_n$-R.

spacing of 0.225 nm associated with the (110) plane of the cubic phase of W^0 (Figure S11). Furthermore, some W agglomeration was also discerned by EDS elemental mapping.

The structural modifications of the recycled catalyst were also investigated by XPS (Figure 6b–d). The W 4f core-level XPS spectrum revealed an increase in the components associated with W(IV) at the expense of those of tungsten oxysulfide species ($W^VO_xS_y$), while the W^0-associated components remain practically unchanged. This means that trinuclear tungsten units, which were partially oxidized in the preparation of the nanomaterial $\{Mo_{2.89}W_{0.11}S_4\}_n$, are reduced to W(IV) again, thus decreasing the degree of oxysulfide species. Moreover, this XPS result also confirms that the W_3S_4 cluster unit within the nanomaterial $\{Mo_{2.89}W_{0.11}S_4\}_n$ remains stable under the catalytic reaction conditions, and, therefore, that the increase in the particle size of W^0 (detected by XRD) is due to agglomeration rather than to a further reductive decomposition of the W_3S_4 constituent units.

Thus, since the W^0 content of the fresh and the recycled catalyst is the same, it is obvious that the recycled catalyst containing larger W^0 nanoparticles should display W^0 atoms on the surface to a lesser extent. At this point, it is worth mentioning that the de(hydrogenation) activity of metal nanoparticles is usually directly correlated with the accessible metal

sites located at the particle surface. Consequently, the fact that no catalyst deactivation occurred along the reaction runs, in which agglomeration of W^0 takes place, suggests that the W^0 particles act as merely spectators in the catalytic process.

The signal deconvolution in the high-resolution S 2p energy-level spectrum unveiled other relevant structural modification. Concretely, a small decrease in the area ratio of unsaturated bridging to saturated sulfur species (red and blue color in Figure 2a, respectively) was detected. The variation in the sulfur content was also confirmed by ICP-OES measurements combined with elemental analysis, which resulted in a slightly lower S/(Mo + W) molar ratio in the recycled catalyst compared to that of the fresh one (1.23 versus 1.33, respectively). Interestingly, the subtle vanishing of the unsaturated bridging sulfurs suggests that these species could be directly involved in the borrowing hydrogen process, most likely as basic Lewis sites where sulfhydryl species (S–H) are formed by alcohol dehydrogenation, as proposed for the monometallic catalyst $\{Mo_3S_4\}_n$ in our previous work.[69]

Catalyst-Centered Borrowing Hydrogen Process: Probing into the Active Sites

It is well established that, in a borrowing hydrogen process involving alcohols, the catalyst should be able to dehydrogenate the alcohol to aldehyde, to promote the formation of the transient unsaturated intermediate, and to carry out the reduction of this intermediate by transfer hydrogenation (see Scheme 1a). In order to demonstrate that $\{Mo_{2.89}W_{0.11}S_4\}_n$ acts as a catalyst in which hydrogen species derived from alcohols are formed on its surface and transferred, a two-step experiment for the model reaction was conducted. First, after the pre-activation treatment, the catalyst $\{Mo_{2.89}W_{0.11}S_4\}_n$ was reacted with benzyl alcohol (**2a**) under neat conditions, thoroughly washed, and dried. Then, the recovered catalyst was used for the direct thiolation of benzaldehyde (**2a′**) with benzenethiol (**1a**), which is the reaction that corresponds to the second step of the overall borrowing hydrogen thioetherification of alcohols shown in Scheme 2 (for more details see Scheme S1). Gratifyingly, the desired thioether **3aa** was obtained in 18% yield, whereas only 6% was yielded when the reaction was run in the presence of the catalyst $\{Mo_{2.89}W_{0.11}S_4\}_n$ without having been previously used for the alcohol dehydrogenation reaction step. The residual catalytic performance (6% yield of **3aa**) of the non-alcohol-treated catalyst is likely to originate from the presence of sulfhydryl (S—H) species derived from the decomposition of hydrazine ligands remaining in the catalyst structure after its preparation.

To obtain further insights on the nature of the active species involved in the borrowing hydrogen process, in situ IR spectroscopy studies were undertaken (Figure 7a and Figure S12). After dosing benzyl alcohol (**2a**) on the catalyst $\{Mo_{2.89}W_{0.11}S_4\}_n$, which had been previously pre-treated at 80 °C under vacuum for 2 h, the temperature was increased up to 180 °C. A broad band centered at 2173 cm^{-1} emerged together with the appearance of a broad shoulder centered approximately at 1652 cm^{-1}. These IR bands are respectively associated with the vibrational frequencies of sulfhydryl (S—H) and metal hydride (M—H; M=Mo, W) species,[69,100] whose formation could arise from the alcohol to aldehyde dehydrogenation. Interestingly, by cooling down to room temperature, this latter IR band became broader and more intense, and its deconvolution and fitting revealed the presence of two additional bands, one centered at 1678 cm^{-1} while the other one appears centered at lower vibrational frequencies (1632 cm^{-1}). These two new IR bands can be ascribed to the vibration of the carbonyl bond (C=O), and, therefore, their appearing suggests that the dehydrogenation product, i.e. benzaldehyde (**2a′**), is re-adsorbed on two type of acid sites of the catalyst surface that display different acidic properties. The higher the acidity of the metal, the lower the strength of the carbonyl bond (C=O). Thus, the IR band at higher vibrational frequencies (1678 cm^{-1}) is associated with the re-adsorption of **2a′** on Mo(IV) centers, whereas the band at 1632 cm^{-1} is likely due to the interaction of **2a′** with more acidic W(IV) species. Finally, before finishing the in situ IR experiment, the sample was subjected to high vacuum conditions, whereby the C=O vibrational bands disappeared while the M—H band
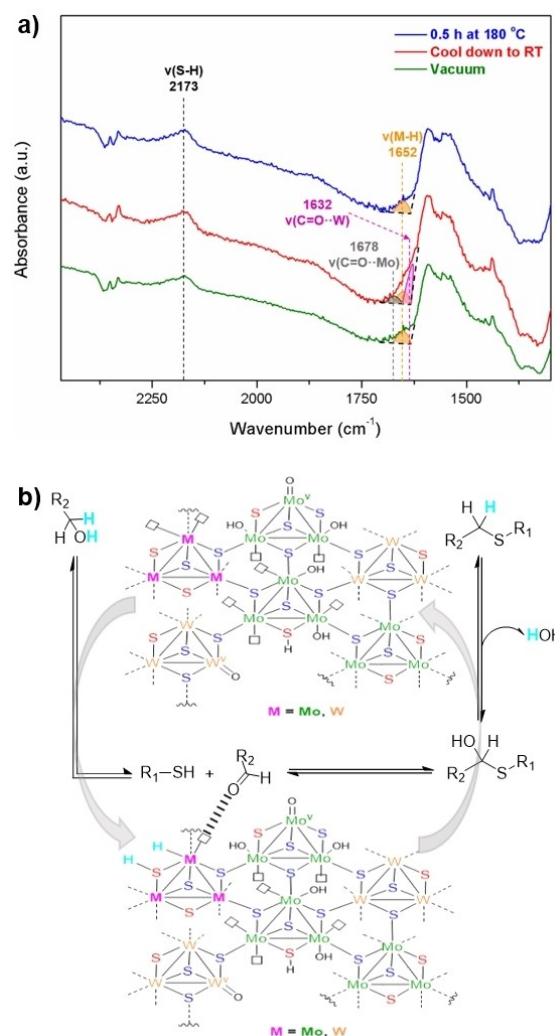
Figure 7. a) IR spectra of $\{Mo_{2.89}W_{0.11}S_4\}_n$ showing the evolution of the bands after dosing benzyl alcohol (**2a**) and sequentially heating to 180 °C (blue), cooling down to room temperature (red), followed by vacuum (green). **b)** Plausible mechanism for the borrowing hydrogen thioetherification of alcohols in the presence of the activated catalyst $\{Mo_{2.89}W_{0.11}S_4\}_n$.

was maintained, thus inferring that the metal hydride species are relatively stable.

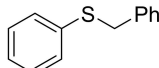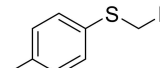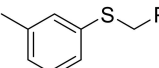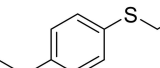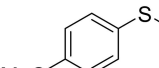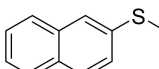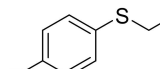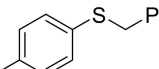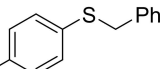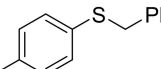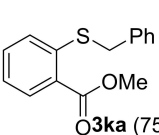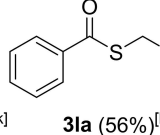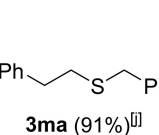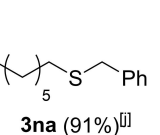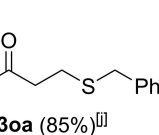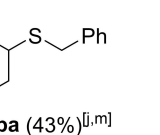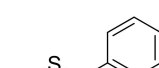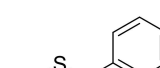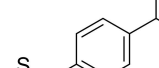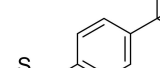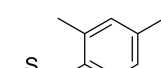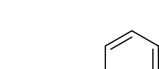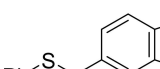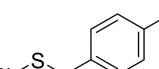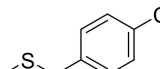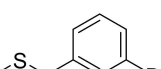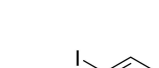Based on all catalytic and characterization results, including the recycling experiments and the in situ IR spectroscopy study, it can be concluded that the alcohol to aldehyde dehydrogenation presumably occurs on coordinatively unsaturated sulfides, i.e. bridging sulfides, and metal centers, forming sulfhydryl (S—H) and metal hydride (M—H; M=Mo, W) species. In addition, it is also revealed that vacant coordination sites around both Mo(IV) and W(IV) metal centers play a key role as Lewis acid sites adsorbing/activating the aldehyde intermediate by interaction through the carbonyl group, thus promoting the nucleophilic attack of the thiol. Subsequently, the transfer hydrogenation of the alcohol-derived hydrogen species (S—H and M—H) from the catalyst to the presumably formed transient hemithioacetal affords the expected thioether product (Figure 7b).

ChemSusChem

Research Article
doi.org/10.1002/cssc.202500343

Chemistry Europe
European Chemical
Societies Publishing

Substrate Scope

The substrate scope for the borrowing hydrogen thioetherification of alcohols in the presence of the catalyst {Mo$_{2.89}$W$_{0.11}$S$_4$}$_n$ was investigated by reaction of structurally diverse thiols (1a–1p) with different alcohols (2a–2p) under standard conditions (Table 1). Thioethers 3ba-3fa were obtained in high yields (82-99%) by reaction of benzyl alcohol (2a) with aryl thiols functionalized with alkyl, methoxy, or a benzene-fused aromatic ring (1b–1f). Similarly, halogen-substituted thiols also displayed good reactivity towards the formation of the desired halogenated thioethers (3ga–3ia). No dehalogenation-side reactions were detected by using the fluorine- and chlorine- substituted

thiols, and 3ga and 3ha were isolated in around 90% yield. In the case of the bromine-containing thiol (1i), the dehalogenated-side product of this reaction, i.e. 3aa, was only formed in a negligible yield (<1%), and the corresponding thioether 3ia could be isolated in 81% yield. Interestingly, nitrile, ester, and thioester groups were also well tolerated under reaction conditions, so that the thioethers 3ja–3la containing these reducible functionalities were achieved in satisfactory yields. Aliphatic thiols showed slightly lower reactivity, which could be overcome by increasing the catalyst loading. Indeed, excellent yields were obtained for thioethers formed by reaction between the alcohol 2a and linear aliphatic thiols, even with those containing phenyl and easily reducible ester groups (3ma–3oa).

Table 1. Borrowing hydrogen synthesis of thioethers catalyzed by {Mo$_{2.89}$W$_{0.11}$S$_4$}$_n$.[a]

$$R^1\text{-SH} + HO\diagup R^2 \xrightarrow[\text{Toluene, 16 h}]{\substack{\{Mo_{2.89}W_{0.11}S_4\}_n \\ \text{10 bar } N_2, \ 180\ ^\circ C}} R^1\diagdown S\diagup R^2 + R^1\diagdown S\diagdown S\diagup R^1$$

1a-p[b]   2a-p   3aa-pa; 3ab-ap[c]   4a-p[d]

3aa (94%)	3ba (99%)	3ca (79%)[e]	3da (85%)[f]	3ea (83%)[g]
3fa (80%)[h]	3ga (89%)	3ha (91%)	3ia (81%)[g,i]	3ja (62%)[j]
3ka (75%)[k]	3la (56%)[l]	3ma (91%)[j]	3na (91%)[j]	3oa (85%)[j]	3pa (43%)[j,m]
3ab (87%)	3ac (91%)	3ad (92%)	3ae (77%)	3af (78%)
3ag (99%)	3ah (88%)[n]	3ai (68%)[o]	3aj (86%)[p]	3ak (88%)[q]
3al (84%)[r]	3am (80%)[s]	3an (92%)[t]	3ao (95%)[u]	3ap (54%)[v]

[a] Catalyst activation: 180°C, 2 h, vacuum; Reaction conditions: 1a–o (0.25 mmol), 2a–p (0.75 mmol), {Mo$_{2.89}$W$_{0.11}$S$_4$}$_n$ (34 mg), toluene (3 mL), 10 bar N$_2$, 180°C, 16 h. [b] Conversion determined by GC using n-hexadecane as an internal standard. [c] Yield of isolated products is given with full conversion of thioethers unless otherwise stated. [d] Yield determined by GC using n-hexadecane as an internal standard. [e] 88% conv. [f] 86% conv. [g] {Mo$_{2.89}$W$_{0.11}$S$_4$}$_n$ (40 mg). [h] {Mo$_{2.89}$W$_{0.11}$S$_4$}$_n$ (50 mg). [i] <1% yield 3aa. [j] {Mo$_{2.89}$W$_{0.11}$S$_4$}$_n$ (68 mg). [k] 2-(benzylthio)benzoic acid detected as a side-product. [l] phenyl-lmethanethiol detected as a by-product. [m] 45% conv. [n] 3% yield 4a. [o] 2% yield 4a. [p] 94% conv.; 1% yield 4a. [q] 91% conv.; 1% yield 4a. [r] 2% yield 4a; 5% yield 3aa. [s] 81% conv. 2% yield 4a. [t] 3% yield 4a. [u] 98% conv.; [v] 16% yield 4a.

ChemSusChem

Research Article
doi.org/10.1002/cssc.202500343

Chemistry Europe
European Chemical
Societies Publishing

However, moderate efficiency was observed for the thioetherification of **2a** with cyclohexanethiol to obtain the corresponding aliphatic thioether **3pa**.

Next, we investigated the thioetherification of different alcohols with benzenethiol (**1a**). The use of 2-naphthalenemethanol (**2b**) afforded the corresponding thioether **3ab** in 87% yield. Benzyl alcohols containing alkyl substituents resulted to be excellent reactants towards the formation of the desired thioethers **3ac–3af**, which were achieved in up to 92% isolated yield. Likewise, the electron-rich benzyl alcohols **2g** and **2h** also displayed excellent reactivity, resulting in the corresponding thioethers **3ag** and **3ah** in 99 and 88% yields, respectively. In the case of using benzyl alcohols that have electron-withdrawing substituents, such as trifluoromethyl (**2i**) and halogens (**2j**–**2l**), a slight decrease in the reaction efficiency was observed. Since it has been established that in the presence of the catalyst $\{Mo_{2.89}W_{0.11}S_4\}_n$ the reductive thiolation between the aldehyde intermediate and the thiol is the rate determining-step, the decrease in activity is likely due to these electron-withdrawing groups limit the ability of the aldehyde intermediate to be adsorbed/activated on vacant coordination metal sites with Lewis acid character. Nonetheless, the halogenated thioethers could be isolated in 84–88% yield (**3aj**–**3al**), thus showing that the halogen groups were well tolerated. Moderate reactivity was reached when an ester-functionalized benzyl alcohol was used, but, gratifyingly, this reducible group was completely retained, yielding the desired thioether **3am** in 80% yield. The non-benzylic-type heterocyclic alcohol **2n** also underwent the thioetherification reaction in 92% yield under isolation. However, in case of using non-activated aliphatic alcohols, such as 1-decanol, low reactivity toward the desired thioether was achieved (Scheme S2). Furthermore, this catalytic methodology could be also extended to the use of more challenging secondary alcohols allowing the preparation of the thioethers **3ao** and **3ap**. On the contrary, when benzenethiol (**1a**) was reacted with 2-phenyl-2-propanol, which is a tertiary benzylic alcohol that easily generates the corresponding carbocation, the desired thioether was only obtained in 12% yield (Scheme S3). Importantly, this result further supports that the thioetherification of alcohols in the presence of $\{Mo_{2.89}W_{0.11}S_4\}_n$ proceeds through a borrowing hydrogen mechanism, ruling out the possibility that it occurs by a direct nucleophiolic substitution in which carbocation intermediates are formed.

Conclusions

In summary, we have prepared a series of molybdenum and tungsten sulfides bimetallic nanomaterials by reacting isostructural molecular complexes with M_3S_4 (M=Mo, W) cluster cores in a reducing aqueous media. Their catalytic performance has been investigated for the thioetherification of benzyl alcohol (**2a**) with benzenethiol (**1a**) to afford benzyl phenyl sulfide (**3aa**) through a borrowing hydrogen synthetic strategy. The comparative catalytic study has found that the yield of the target thioether product **3aa** presents a volcano dependence with the W/Mo mole ratio. Kinetic studies have shown that the presence

of tungsten accelerates the alcohol dehydrogenation step. The characterization results have revealed that the most active catalyst, namely $\{Mo_{2.89}W_{0.11}S_4\}_n$, is constituted by randomly agglomerated nanosheets of amorphous nature exhibiting irregular and disordered alloyed basal planes, which are formed by assembled molecular M_3S_4 (M=Mo, W) cluster units. In addition, W^0 species derived from the partial reductive decomposition of the W_3S_4 molecular precursor are also present to a lesser extent. However, based on all catalytic and characterization results, including the in situ IR spectroscopy study, the borrowing hydrogen activity of $\{Mo_{2.89}W_{0.11}S_4\}_n$ has been ascribed to the presence of coordinatively unsaturated bridging sulfide ligands and vacant coordination sites around both Mo(IV) and W(IV) metal centers, whereas W^0 species act as merely spectators. In particular, both types of actives centers, respectively displaying Lewis basic and Lewis acid properties, participate in the alcohol-to-aldehyde dehydrogenation step forming sulfhydryl (S–H) and metal hydride (M–H; M=Mo, W) species. Furthermore, the Lewis acid molybdenum and tungsten metal centers are also crucial for promoting the reductive thiolation step.

It has been demonstrated that $\{Mo_{2.89}W_{0.11}S_4\}_n$ presents good recyclability and is of broad scope. Indeed, its applications has allowed the synthesis of a wide variety of thioethers, even bearing halogen, nitrile, esters, and thioamide sensitive functional groups, from structurally diverse thiols and primary as well as secondary alcohols. Importantly, this work may pay the way for the activation of the basal planes of MoS_2-derived materials by allowing engineering to be applied as catalysts in the design of atom-economical, practical, and, in general, more sustainable synthetic strategies for other value-added fine chemicals.

Supporting Information

The Supporting Information includes: General information on techniques used for characterization, experimental procedures employed for the preparation of catalysts and catalytic experiments, extended catalytic data of the kinetic studies for the borrowing hydrogen thioetherification of alcohols, additional XPS characterization data, kinetic data and characterization of the recycled catalyst $\{Mo_{2.89}W_{0.11}S_4\}_n$-R, extended catalytic data for the $\{Mo_{2.89}W_{0.11}S_4\}_n$-catalyzed borrowing hydrogen thioetherification of alcohols, complementary IR spectra, extension of scope, and characterization data and NMR spectra of the isolated thioethers. The authors have cited additional references within the Supporting Information.[70,105] Raw research data from this work are published in an open-access repository.[106]

ChemSusChem

Research Article
doi.org/10.1002/cssc.202500343

Chemistry Europe
European Chemical
Societies Publishing

Conflict of Interests

The authors declare no conflict of interest.

Data Availability Statement

The data that support the findings of this study are openly available in Mendeley Data at https://data.mendeley.com/datasets/3z4k468n25/1, reference number 0.

Keywords: alloyed molybdenum-tungsten sulfides · borrowing hydrogen catalysis · C—S bond formation · alcohols · thioethers

[1] S. Patai, in *The Chemistry of the Functional Groups- The Chemistry of the Thiol Group*, Wiley, London, **1974**.

[2] F. Bernardi, I. G. Csizmadia, A. Mangini, in *Organic Sulfur Chemistry. Theoretical and Experimental Advances*, Elsevier, Amsterdam, **1985**.

[3] R. J. Cremlyn, in *An Introduction to Organosulfur Chemistry*, John Wiley & Sons, New York, **1996**.

[4] T. Kondo, T.-a. Mitsudo, *Chem. Rev.* **2000**, *100*, 3205–3220.

[5] H. Liu, X. Jiang, *Chem. Asian J.* **2013**, *8*, 2546–2563.

[6] C. Shen, P. Zhang, Q. Sun, S. Bai, T. S. A. Hor, X. Liu, *Chem. Soc. Rev.* **2015**, *44*, 291–314.

[7] D. P. Nair, M. Podgórski, S. Chatani, T. Gong, W. Xi, C. R. Fenoli, C. N. Bowman, *Chem. Mater.* **2014**, *26*, 724–744.

[8] M. Feng, B. Tang, S. H. Liang, X. Jiang, *Curr. Top. Med. Chem.* **2016**, *16*, 1200–1216.

[9] Z. Qiao, X. Jiang, *Org. Biomol. Chem.* **2017**, *15*, 1942–1946.

[10] E. A. Ilardi, E. Vitaku, J. T. Njardarson, *J. Med. Chem.* **2014**, *57*, 2832–2842.

[11] L. Dong, B. Song, J. Wu, Z. Wu, Y. Zhu, X. Chen, D. Hu, *Phosphorus Sulfur Silicon Relat. Elem.* **2016**, *191*, 904–907.

[12] Y. Guo, X. Wang, J. Fan, Q. Zhang, Y. Wang, Y. Zhao, M. Huang, M. Ding, Y. Zhang, *R. Soc. Open Sci.* **2017**, *4*, 171053.

[13] J. Shi, N. Luo, M. Ding, X. Bao, *Chin. Chem. Lett.* **2020**, *31*, 434–438.

[14] B. Xu, Y. Lin, Y. Ye, L. Xu, T. Xie, X.-Y. Ye, *RSC Adv.* **2022**, *12*, 692–697.

[15] A. R. Jadhao, S. S. Gaikwad, *J. Org. Chem.* **2023**, *88*, 14078–14087.

[16] X. Ma, H. Jin, M. Zeng, Y. Qin, L. Tan, T. Miao, Y. Feng, Q. Shi, *Eur. J. Org. Chem.* **2023**, *26*, e202300702.

[17] K.-i. Shimizu, *Catal. Sci. Technol.* **2015**, *5*, 1412–1427.

[18] A. Corma, J. Navas, M. J. Sabater, *Chem. Rev.* **2018**, *118*, 1410–1459.

[19] H. P., S. Hati, R. Dey, *Org. Biomol. Chem.* **2023**, *21*, 6360–6367.

[20] A. Corma, J. Navas, T. Ródenas, M. J. Sabater, *Chem. Eur. J.* **2013**, *19*, 17464–17471.

[21] R. S. Glass, *Synth. Commun.* **1976**, *6*, 47–51.

[22] Y. Kikugawa, *Chem. Lett.* **1981**, 1157–1158.

[23] G. A. Olah, Q. Wang, N. J. Trivedi, G. K. Surya Prakash, *Synthesis* **1992**, 465–466.

[24] G. A. Olah, Q. Wang, X.-y. Li, G. K. Surya Prakash, *Synlett* **1993**, 32–34.

[25] L. Li, Y. Ding, *Mini-Rev. Org. Chem.* **2017**, *14*, 407–431.

[26] H. B. Glass, E. E. Reid, *J. Am. Chem. Soc.* **1929**, *51*, 3428–3430.

[27] G. Dougherty, P. D. Hammond, *J. Am. Chem. Soc.* **1935**, *57*, 117–118.

[28] M. Kosugi, T. Ogata, M. Terada, H. Sano, T. Migita, *Bull. Chem. Soc. Jpn.* **1985**, *58*, 3657–3658.

[29] J. Yin, C. Pidgeon, *Tetrahedron Lett.* **1997**, *38*, 5953–5954.

[30] J. F. Hartwig, *Acc. Chem. Res.* **2008**, *41*, 1534–1544.

[31] P. Bichler, J. A. Love, in *C–X Bond Formation* (Ed.: A. Vigalok), Springer Berlin Heidelberg, Berlin, Heidelberg, **2010**, pp. 39–64.

[32] I. P. Beletskaya, V. P. Ananikov, *Chem. Rev.* **2011**, *111*, 1596–1636.

[33] C. C. Eichman, J. P. Stambuli, *Molecules* **2011**, *16*, 590–608.

[34] C. Uyeda, Y. Tan, G. C. Fu, J. C. Peters, *J. Am. Chem. Soc.* **2013**, *135*, 9548–9552.

[35] A. M. Wagner, M. S. Sanford, *J. Org. Chem.* **2014**, *79*, 2263–2267.

[36] M. Jouffroy, C. B. Kelly, G. A. Molander, *Org. Lett.* **2016**, *18*, 876–879.

[37] M. S. Oderinde, M. Frenette, D. W. Robbins, B. Aquila, J. W. Johannes, *J. Am. Chem. Soc.* **2016**, *138*, 1760–1763.

[38] B. Liu, C.-H. Lim, G. M. Miyake, *J. Am. Chem. Soc.* **2017**, *139*, 13616–13619.

[39] M. M. Talukder, J. T. Miller, J. M. O. Cue, C. M. Udamulle, A. Bhadran, M. C. Biewer, M. C. Stefan, *Organometallics* **2021**, *40*, 83–94.

[40] P. Kumar, R. K. Pandey, V. R. Hegde, *Synlett* **1999**, 1921–1922.

[41] S. Kanagasabapathy, A. Sudalai, B. C. Benicewicz, *Tetrahedron Lett.* **2001**, *42*, 3791–3794.

[42] N. Morita, N. Krause, *Angew. Chem. Int. Ed.* **2006**, *45*, 1897–1899.

[43] M. Kawatsura, Y. Komatsu, M. Yamamoto, S. Hayase, T. Itoh, *Tetrahedron Lett.* **2007**, *48*, 6480–6482.

[44] S. Banerjee, J. Das, R. P. Alvarez, S. Santra, *New J. Chem.* **2010**, *34*, 302–306.

[45] J. R. Cabrero-Antonino, A. Leyva-Pérez, A. Corma, *Adv. Synth. Catal.* **2012**, *354*, 678–687.

[46] J. R. Cabrero-Antonino, A. Leyva-Pérez, A. Corma, *Chem. Eur. J.* **2013**, *19*, 8627–8633.

[47] R. Castarlenas, A. Di Giuseppe, J. J. Pérez-Torrente, L. A. Oro, *Angew. Chem. Int. Ed.* **2013**, *52*, 211–222.

[48] X. Zeng, *Chem. Rev.* **2013**, *113*, 6864–6900.

[49] K. Kuciński, P. Pawluć, G. Hreczycho, *Adv. Synth. Catal.* **2015**, *357*, 3936–3942.

[50] R. Kumar, Saima, A. Shard, N. H. Andhare, Richa, A. K. Sinha, *Angew. Chem. Int. Ed.* **2015**, *54*, 828–832.

[51] M. Pérez, T. Mahdi, L. J. Hounjet, D. W. Stephan, *Chem. Commun.* **2015**, *51*, 11301–11304.

[52] L. Palacios, A. Di Giuseppe, M. J. Artigas, V. Polo, F. J. Lahoz, R. Castarlenas, J. J. Pérez-Torrente, L. A. Oro, *Catal. Sci. Technol.* **2016**, *6*, 8548–8561.

[53] J. L. Kennemur, G. D. Kortman, K. L. Hull, *J. Am. Chem. Soc.* **2016**, *138*, 11914–11919.

[54] L. Palacios, Y. Meheut, M. Galiana-Cameo, M. J. Artigas, A. Di Giuseppe, F. J. Lahoz, V. Polo, R. Castarlenas, J. J. Pérez-Torrente, L. A. Oro, *Organometallics* **2017**, *36*, 2198–2207.

[55] J. R. Cabrero-Antonino, M. Tejeda-Serrano, M. Quesada, J. A. Vidal-Moya, A. Leyva-Pérez, A. Corma, *Chem. Sci.* **2017**, *8*, 689–696.

[56] M. T. Martin, A. M. Thomas, D. G. York, *Tetrahedron Lett.* **2002**, *43*, 2145–2147.

[57] B. P. Bandgar, S. S. Gawande, D. B. Muley, *Green Chem. Lett. Rev.* **2010**, *3*, 49–54.

[58] K. Bahrami, M. M. Khodaei, N. Khodadoustan, *Synlett* **2011**, 2206–2210.

[59] B. Basu, S. Kundu, D. Sengupta, *RSC Adv.* **2013**, *3*, 22130–22134.

[60] H. Hikawa, M. Toyomoto, S. Kikkawa, I. Azumaya, *Org. Biomol. Chem.* **2015**, *13*, 11459–11465.

[61] H. Hikawa, Y. Machino, M. Toyomoto, S. Kikkawa, I. Azumaya, *Org. Biomol. Chem.* **2016**, *14*, 7038–7045.

[62] F. Santoro, M. Mariani, F. Zaccheria, R. Psaro, N. Ravasio, *Beilstein J. Org. Chem.* **2016**, *12*, 2627–2635.

[63] K. Kucinski, G. Hreczycho, *Eur. J. Org. Chem.* **2017**, 5572–5581.

[64] M. Markwitz, K. Labrzycki, L. Azcune, A. Landa, K. Kuciński, *Sci. Rep.* **2023**, *13*, 20624.

ChemSusChem

Research Article

doi.org/10.1002/cssc.202500343

Chemistry Europe
European Chemical
Societies Publishing

[65] J. Li, J. Ma, C. Wei, Z. Zheng, Y. Han, H. Wang, X. Wang, C. Hu, *Dalton Trans.* **2024**, *53*, 4492–4500.

[66] I. Sorribes, L. Liu, A. Corma, *ACS Catal.* **2017**, *7*, 2698–2708.

[67] I. Sorribes, L. Liu, A. Doménech-Carbó, A. Corma, *ACS Catal.* **2018**, *8*, 4545–4557.

[68] I. Sorribes, A. Corma, *Chem. Sci.* **2019**, *10*, 3130–3142.

[69] M. Rodenes, F. Dhaeyere, S. Martín, P. Concepción, A. Corma, I. Sorribes, *ACS Sustainable Chem. Eng.* **2023**, *11*, 12265–12279.

[70] M. Rodenes, F. Gonell, S. Martín, A. Corma, I. Sorribes, *JACS Au* **2022**, *2*, 601–612.

[71] B. Seo, S. H. Joo, *Nano Convergence* **2017**, *4*, 19.

[72] C. Wu, J. Zhang, X. Tong, P. Yu, J.-Y. Xu, J. Wu, Z. M. Wang, J. Lou, Y.-L. Chueh, *Small* **2019**, *15*, 1900578.

[73] X. Zhang, F. Jia, S. Song, *Chem. Eng. J.* **2021**, *405*, 127013.

[74] S. Singh, A. Modak, K. K. Pant, A. Sinhamahapatra, P. Biswas, *ACS Appl. Nano Mater.* **2021**, *4*, 8644–8667.

[75] P. P. Singh, S. Sinha, G. Pandey, V. Srivastava, *RSC Adv.* **2022**, *12*, 29826–29839.

[76] X. Zhang, S. Hua, L. Lai, Z. Wang, T. Liao, L. He, H. Tang, X. Wan, *RSC Adv.* **2022**, *12*, 17959–17983.

[77] R. Li, J. Liang, T. Li, L. Yue, Q. Liu, Y. Luo, M. S. Hamdy, Y. Sun, X. Sun, *Chem. Commun.* **2022**, *58*, 2259–2278.

[78] X. Zhang, B. Chen, J. Wang, Y. Zhou, X. Huang, H. Huang, X. Wang, K. Li, *ACS Omega* **2023**, *8*, 18400–18407.

[79] M. Saliba, J. P. Atanas, T. M. Howayek, R. Habchi, *Nanoscale Adv.* **2023**, *5*, 6787–6803.

[80] J. V. Lauritsen, M. Nyberg, J. K. Norskov, B. S. Clausen, H. Topsoe, E. Laegsgaard, F. Besenbacher, *J. Catal.* **2004**, *224*, 94–106.

[81] J. V. Lauritsen, J. Kibsgaard, G. H. Olesen, P. G. Moses, B. Hinnemann, S. Helveg, J. K. Nørskov, B. S. Clausen, H. Topsøe, E. Lægsgaard, F. Besenbacher, *J. Catal.* **2007**, *249*, 220–233.

[82] H. Topsøe, *Appl. Catal. A* **2007**, *322*, 3–8.

[83] G. Berhault, M. Perez De la Rosa, A. Mehta, M. J. Yácaman, R. R. Chianelli, *Appl. Catal. A* **2008**, *345*, 80–88.

[84] F. Besenbacher, M. Brorson, B. S. Clausen, S. Helveg, B. Hinnemann, J. Kibsgaard, J. V. Lauritsen, P. G. Moses, J. K. Nørskov, H. Topsøe, *Catal. Today* **2008**, *130*, 86–96.

[85] J. Kibsgaard, A. Tuxen, K. G. Knudsen, M. Brorson, H. Topsøe, E. Lægsgaard, J. V. Lauritsen, F. Besenbacher, *J. Catal.* **2010**, *272*, 195–203.

[86] Y. Zhu, Q. M. Ramasse, M. Brorson, P. G. Moses, L. P. Hansen, C. F. Kisielowski, S. Helveg, *Angew. Chem. Int. Ed.* **2014**, *53*, 10723–10727.

[87] S. Rangarajan, M. Mavrikakis, *ACS Catal.* **2016**, *6*, 2904–2917.

[88] L. S. Byskov, B. Hammer, J. K. Norskov, B. S. Clausen, H. Topsoe, *Catal. Lett.* **1997**, *47*, 177–182.

[89] J. V. Lauritsen, M. V. Bollinger, E. Lægsgaard, K. W. Jacobsen, J. K. Nørskov, B. S. Clausen, H. Topsøe, F. Besenbacher, *J. Catal.* **2004**, *221*, 510–522.

[90] B. Hinnemann, P. G. Moses, J. Bonde, K. P. Jørgensen, J. H. Nielsen, S. Horch, I. Chorkendorff, J. K. Nørskov, *J. Am. Chem. Soc.* **2005**, *127*, 5308–5309.

[91] T. F. Jaramillo, K. P. Jorgensen, J. Bonde, J. H. Nielsen, S. Horch, I. Chorkendorff, *Science* **2007**, *317*, 100–102.

[92] L. P. Hansen, Q. M. Ramasse, C. Kisielowski, M. Brorson, E. Johnson, H. Topsøe, S. Helveg, *Angew. Chem. Int. Ed.* **2011**, *50*, 10153–10156.

[93] J. Kibsgaard, Z. Chen, B. N. Reinecke, T. F. Jaramillo, *Nat. Mater.* **2012**, *11*, 963–969.

[94] D. Kong, H. Wang, J. J. Cha, M. Pasta, K. J. Koski, J. Yao, Y. Cui, *Nano Lett.* **2013**, *13*, 1341–1347.

[95] Z. He, W. Que, *Appl. Mater. Today* **2016**, *3*, 23–56.

[96] F. Gonell, M. Rodenes, S. Martín, M. Boronat, I. Sorribes, A. Corma, *Chem. Mater.* **2023**, *35*, 8483–8493.

[97] J.-G. Song, G. H. Ryu, S. J. Lee, S. Sim, C. W. Lee, T. Choi, H. Jung, Y. Kim, Z. Lee, J.-M. Myoung, C. Dussarrat, C. Lansalot-Matras, J. Park, H. Choi, H. Kim, *Nat. Commun.* **2015**, *6*, 7817.

[98] A. Majid, Z. Ghaffar, U. A. Rana, S. U.-D. Khan, M. Yoshiya, *Comput. Theor. Chem.* **2016**, *1084*, 98–102.

[99] P. D. Tran, T. V. Tran, M. Orio, S. Torelli, Q. D. Truong, K. Nayuki, Y. Sasaki, S. Y. Chiam, R. Yi, I. Honma, J. Barber, V. Artero, *Nat. Mater.* **2016**, *15*, 640.

[100] Y. Deng, L. R. L. Ting, P. H. L. Neo, Y.-J. Zhang, A. A. Peterson, B. S. Yeo, *ACS Catal.* **2016**, *6*, 7790–7798.

[101] F. D. Hardcastle, I. E. Wachs, *J. Raman Spectrosc.* **1990**, *21*, 683–691.

[102] D. Escalera-López, Z. Lou, N. V. Rees, *Adv. Energy Mater.* **2019**, *9*, 1802614.

[103] G. E. McGuire, G. K. Schweitzer, T. A. Carlson, *Inorg. Chem.* **1973**, *12*, 2450–2453.

[104] M. Morant-Giner, I. Brotons-Alcázar, N. Y. Shmelev, A. L. Gushchin, L. T. Norman, A. N. Khlobystov, A. Alberola, S. Tatay, J. Canet-Ferrer, A. Forment-Aliaga, E. Coronado, *Chem. Eur. J.* **2020**, *26*, 6670–6678.

[105] M. N. Sokolov, S. A. Adonin, A. V. Virovets, P. A. Abramov, C. Vicent, R. Llusar, V. P. Fedin, *Inorg. Chim. Acta* **2013**, *395*, 11–18.

[106] M. Rodenes, D. Oštrić, S. Martín, P. Concepción, A. Corma, I. Sorribes, *Mendeley Data, V1* **2024**, 10.17632/3z4k468n25.1.